Marine Pollution Bulletin 209 (2024) 117190

Contents lists available at ScienceDirect

Marine Pollution Bulletin

journal homepage: www.elsevier.com/locate/marpolbul

Labile organic matter favors a low N_2O yield during nitrogen removal in estuarine sediments

Ehui Tan [a,*], Bin Chen [b], Lili Han [a], Wenbin Zou [b], Xiuli Yan [c], Zhixiong Huang [a], Yu Han [a], Zhenzhen Zheng [a], Liwei Zheng [a], Min Xu [a], Jin-Yu Terence Yang [b], Hongyan Bao [b], Shuh-ji Kao [a,b,**]

[a] State Key Laboratory of Marine Resource Utilization in South China Sea, School of Marine Science and Engineering, Hainan University, Haikou, Hainan, China
[b] State Key Laboratory of Marine Environmental Science, Xiamen University, Xiamen, China
[c] Guangdong Provincial Key Laboratory of Marine Disaster Prediction and Prevention, College of Science, Shantou University, Shantou, China

ARTICLE INFO

Keywords:
N_2O production
Denitrification
Labile organic matter
Climatic feedback
Sediment

ABSTRACT

Estuary harbors the active sediment denitrification and nitrous oxide (N_2O) emission, while the knowledge of environmental controls on the denitrification-derived N_2O yield remains underexplored. Here, we quantitatively assess the potential and *in situ* rates of N_2O production during sediment denitrification in the Pearl River Estuary (PRE), China. Organic matter determines the product stoichiometry and capacity of nitrogen removal. In particular, labile organic matter (LOM) reduces N_2O yield *via* enhancing the complete coupled nitrification-denitrification. Our results reveal that the chain processes, primary production-LOM settling-sedimentary respiration-coupled nitrification-denitrification, control the sediment denitrification and N_2O production, linking the carbon and nitrogen biogeochemical cycles in the atmosphere-water column-sediment continuum. The PRE sediments serve as nitrogen removal hotspots but with low efficiency (~25 % of riverine input) and strong N_2O release (~66 % of daily sea-air N_2O efflux). These findings contribute to policy makers to develop knowledge-based management actions for achieving sustainable coastal environments and mitigating N_2O emission.

1. Introduction

Nitrous oxide (N_2O), one of the strong greenhouse gas, is nearly 300 times more potent than carbon dioxide in terms of warming potential at a 100-year horizon, accounting for approximately 8 % of the total radiative effects at a global scale (IPCC, 2021). This long-lived N_2O (~114 years) has become the dominant ozone depleter in the 21st century (Ravishankara et al., 2009). The global atmospheric N_2O concentration has increased continuously from 280 ppb in 1850 to 320 ppb in 2019 with a more rapid annual growth rate over the past decade largely due to the significant anthropogenic interferences (IPCC, 2021). Aquatic environments such as inland/coastal waters are hotspots for N_2O emission contributing to 3.1–5.6 Tg N_2O-N yr^{-1} with a large uncertainty, due to the spatiotemporal heterogeneity of N_2O concentration and the sparse observations (Murray et al., 2015; Tian et al., 2020).

N_2O is known to be an obligate intermediate product along with the stepwise nitrate respiration during denitrification, which is a crucial process for reactive nitrogen (Nr) removal in aquatic ecosystems (Hutchins and Capone, 2022). Coastal sediment harbors the most important site for Nr removal accounting for over 50 % of the global oceanic nitrogen loss (Bohlen et al., 2012), but with a side-effect of strong N_2O release especially in estuarine environments (Jameson et al., 2020; Murray et al., 2015). Standing at the land-ocean continuum, estuary receives a large amount of anthropogenic Nr input and serves as a natural Nr biogeochemical reactor. The global riverine Nr transport to the ocean has been near doubled over the last century (Beusen et al., 2016). In China, the riverine Nr exportation has increased dramatically by 2.7–4.6 folds since 1970s (Wang et al., 2020a). This excess Nr delivery significantly accelerates Nr biogeochemical cycle and associated N_2O release in estuaries, contributing to N_2O budget at both regional and global scales (Katz, 2020; Kessouri et al., 2021).

The size and relative proportion of denitrification-induced N_2O

* Corresponding author.
** Correspondence to: Ehui Tan and Shuh-ji Kao, State Key Laboratory of Marine Resource Utilization in South China Sea, School of Marine Science and Engineering, Hainan University, Haikou, Hainan, China.
E-mail addresses: ehuitan@hainanu.edu.cn (E. Tan), sjkao@hainanu.edu.cn (S.-j. Kao).

https://doi.org/10.1016/j.marpolbul.2024.117190
Received 24 July 2024; Received in revised form 8 October 2024; Accepted 21 October 2024
Available online 24 October 2024

production is largely depended on the completeness of this process and the balance between denitrification and anammox, the other Nr removal pathway with dinitrogen gas (N_2) as the sole product (Hutchins and Capone, 2022). Research on the N_2O production mechanisms and their environmental factors in various ecosystems has become popular in recent years (Ma et al., 2019; Murray et al., 2015; Wan et al., 2023; Xiang et al., 2023; Zhou et al., 2023). Previous studies have indicated that temperature, organic matter (OM), nitrate concentration, water content and pH are key environmental factors regulating N_2O production during denitrification in soil systems (Morley et al., 2014; Phillips et al., 2015; Qu et al., 2014; Senbayram et al., 2012; Wang et al., 2020b). However, the investigations on the sedimentary N_2O production in aquatic ecosystems, especially the N_2O yield and key environmental regulators during denitrification are still underexplored. A better understanding of the product stoichiometry during sediment Nr removal, that is, whether the removed nitrogen flow towards N_2O or N_2 production, will help to coastal N_2O mitigation.

It is widely recognized that labile organic matter (LOM) prefers to sediment denitrification since denitrification is a multi-step and energy-consuming process (Huang et al., 2022; Lai et al., 2022). Spatially, estuarine sediments receive terrestrial OM in the upstream and local-produced LOM in downstream (Yu et al., 2010). We thus hypothesized that the availability of OM determines sediment denitrification-induced N_2O yield and production, with particular LOM stimulates the N_2O reduction resulting in a low proportion of N_2O production. The Pearl River Estuary (PRE) is the second largest estuary in China. The Nr flux delivered *via* the PRE into adjacent coastal waters was 2–2.5 times of that since 1970 (Strokal et al., 2015), resulting in prominent ecological problems, such as eutrophication and seasonal hypoxia (Qian et al., 2022). Moreover, several studies have revealed that the PRE acts as an intensive net N_2O source to atmosphere all year round (Chen et al., 2023; Cheng et al., 2023; Lin et al., 2016). To test our hypothesis, we conducted two campaigns to quantify the potential and *in situ* rates of sediment Nr removal and N_2O production by applying a ^{15}N isotopic pairing technique in the PRE. We confirm that LOM with a low C/N ratio reduces the N_2O yield by promoting the complete denitrification in estuarine sediments.

2. Materials and methods

2.1. Study area

The PRE experiences a subtropical monsoon climate with an average annual temperature of 14–22 °C and a mean annual precipitation of 1200–2200 mm (Zhang et al., 2008). Pearl River, the second largest river in China in terms of discharge, delivers approximately 3.3×10^{11} m^3 yr^{-1} of freshwater and 8.0×10^7 tons yr^{-1} of sediments into the northern South China Sea *via* the PRE (Liu et al., 2009). More than half of sediments were trapped in the PRE, resulting in an area of fine-grained sediments with muddy patches in the north region (Zhang et al., 2013). The PRE is dominated by a semi-diurnal tidal with an average tide height of 1.0–1.7 m (Mao et al., 2004). Previous study has observed a weakening terrestrial OM input seaward and a strengthening contribution from marine OM in surface sediments of the PRE (Yu et al., 2010).

2.2. Sampling and pretreatment

The sampling cruises were conducted onboard R/V "Yuezhanyuke 10" from 13 to 25 July 2020 and from 13 to 28 July 2021, representing the wet season in the PRE. Hydrological investigation, slurry incubation and intact core incubation were conducted in the selected sites during these two campaigns (Fig. 1). The hydrological characteristics, including temperature, salinity and dissolved oxygen (DO) concentration, were measured using the probes embed in a conductivity-temperature-depth (CTD) rosette sampler. The bottom water was collected by applying 12 L Niskin bottles attached on the CTD. One part of water was filtered (0.2 μm) and preserved at −20 °C to measure ammonium (NH_4^+) and nitrate plus nitrite (NO_x^-) concentration; The other ~30 L of bottom water was directly stored in a tank for sediment incubation.

Sediment samples were collected using a box corer (20 × 20 cm), intact cores were then retrieved by inserting PVC tubes (inner diameter: 5 cm and length: 30 cm) after removing the overlying water carefully. The sediment height in intact cores was adjusted into 23 cm. After then, the 2 cm of surface sediments in the box corer were collected for slurry incubation and sediment analysis, including the porosity, Chla concentration, organic carbon (OC) and nitrogen (ON) contents, and carbon isotopic composition.

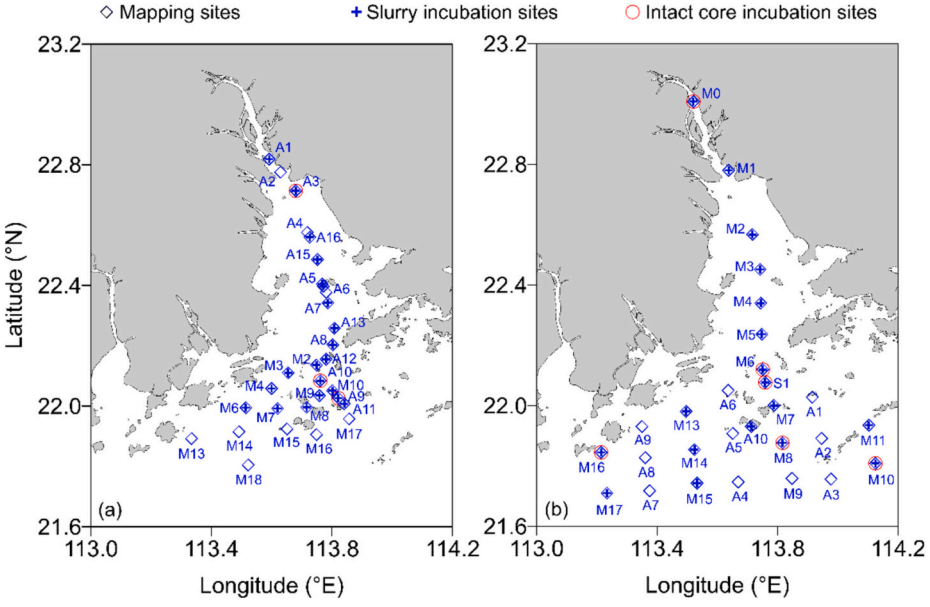

Fig. 1. Map of sampling sites in the Pearl River Estuary during summer in (a) 2020 and (b) 2021.

2.3. Slurry incubation to determine potential biogeochemical rates

The potential rates of Nr removal and N_2O production in the surface sediments were measured *via* slurry incubation (Thamdrup and Dalsgaard, 2002). The surface sediments and the filtered (0.2 μm) bottom water were mixed in 1:4 (*v*/v) ratio to prepare slurry, and then the slurry was deoxygenated by purging He for about 30 min. The DO concentration in slurry was monitored applying an oxygen microsensor. Subsequently, 3 mL of slurry was transferred into 12 mL gas-tight vials (Exetainers, Labco), headspace was replaced with He to ensure an anoxic condition after the vials were capped. All of the slurry samples were pre-incubated in the dark at *in situ* temperature for >24 h to eliminate the background oxygen and NO_x^-. After the pre-incubation, three of the vials were added with 100 μL of saturated $HgCl_2$ solution to measure the residual NO_x^- concentration. The remaining 12 vials were injected by $^{15}NO_3^-$ (Sigma-Aldrich, 98 ^{15}N atom %) to a final concentration of 100 μmol L^{-1} and the slurries were thoroughly mixed. Three vials were then fixed immediately after the ^{15}N tracer addition and assigned as initial. The other 9 vials were fixed within 0.5 h, 1 h and 2 h incubations, respectively. Each time point occupied three vials. The fixed samples were preserved at room temperature before measurement.

2.4. Intact core incubation to determine in situ biogeochemical rates

To avoid the sampling disturbances, the sediment intact cores were equilibrated overnight in a tank with bottom water from the corresponding site, before the determination of sediment oxygen consumption (SOC) rates and *in situ* nitrogen removal rates (Trimmer et al., 2006). The DO concentration in the overlying water was detected before the cores were sealed using Teflon caps with an inlet and an outlet. Then the $^{15}NO_3^-$ (Sigma-Aldrich, 98 ^{15}N atom %) was added into the overlying water *via* the inlet to a concentration gradient (Supplementary Table S1). Each concentration treatment occupied two sediment cores. These cores were pre-incubated for 30 min to allow the added $^{15}NO_3^-$ diffuse into surface sediments (Trimmer et al., 2006). After that, one core in each concentration treatment was randomly selected to stop the incubation, while the remaining cores were incubated for ~2 h at *in situ* temperature and then stopped. To end the incubation, the DO concentration in the overlying water was measured firstly, and then the top 2 cm of sediments were gently mixed with the overlying water (Dalsgaard et al., 2000). The mixed water sample was pipetted to fill a 12 mL gas-tight vial (Exetainer, Labco) prefilled with 100 μL $HgCl_2$. Then 9 mL of sample was discharged by using He gas to create a headspace. The produced ^{15}N-labiled N_2 and N_2O in the remaining samples were all purged into a IRMS and determined. Five replicates were subsampled for each intact core.

2.5. Chemical analysis

The NO_x^- and NH_4^+ concentrations were measured *via* vanadium (III) reduction method (Braman and Hendrix, 1989) and indophenol blue spectrophotometric method (Pai et al., 2001), respectively. The fresh sediments were dried, and 5 mL of 1 N HCl was added to remove inorganic carbon, the OC, ON contents and carbon isotopic composition were analyzed with a EA-IRMS (Kao et al., 2008). The sedimentary Chla concentration was extracted using alcohol (98 %) and then measured applying spectrophotometric method (Pinckney et al., 1994). The DO concentration was measured by using an oxygen microsensor (OX 100, Unisense AS). The oxygen sensor was calibrated in water with a DO saturation of 0 and 100 % before application. The $^{29}N_2$, $^{30}N_2$, $^{45}N_2O$, and $^{46}N_2O$ concentrations in incubation samples were quantified using a GC-IRMS (Thermo Finnigan Delta^{plus} Advantage) (Hsu and Kao, 2013).

2.6. Calculation of potential and in situ nitrogen removal rates

The potential rates of denitrification (D_{total}), anammox (A_{total}), and the associated N_2O production (N_2O_{total}) were quantified according to the slurry incubation (Thamdrup and Dalsgaard, 2002),

$$D_{total} = 2 \times P_{30} \times (r_{14}+1)^2 + (P_{45}+2P_{46}) \times (r_{14}+1), \quad (1)$$

$$A_{total} = (P_{29} - 2 \times r_{14} \times P_{30}) \times (2 \times r_{14}+1), \quad (2)$$

$$N_2O_{total} = 2 \times P_{45} + 2 \times P_{46} \times \left(r_{14}{}^2+1\right), \quad (3)$$

where the P_{29}, P_{30}, P_{45}, and P_{46} represent the production rates of $^{29}N_2$, $^{30}N_2$, $^{45}N_2O$, and $^{46}N_2O$ during the slurry incubation, respectively. r_{14} is the $^{14}NO_3^-/^{15}NO_3^-$ in sediment and is calculated from

$$r_{14} = \frac{C_{14} + 0.02 \times C_{15}}{0.98 \times C_{15}}, \quad (4)$$

where C_{14} is the background NO_x^- concentration after pre-incubation. C_{15} is the added $^{15}NO_3^-$ concentration (100 μmol L^{-1}). The values of 0.02 and 0.98 represent the proportion of ^{14}N and ^{15}N in the added $^{15}NO_3^-$. The relative proportion of anammox to total nitrogen removal (*ra*%) was then calculated,

$$ra\% = 100 \times \frac{A_{total}}{D_{total} + A_{total}}. \quad (5)$$

The SOC rate was calculated by the difference of DO concentration before (DO_{before}) and after (DO_{after}) the intact core incubation:

$$SOC = \frac{(DO_{before} - DO_{after}) \times h}{\Delta T}, \quad (6)$$

where *h* is the height of the overlying water in the intact cores; △T is the incubation time.

The *in situ* rates of denitrification (D_{14}), anammox (A_{14}), denitrification-derived N_2O production (D_{14}-N_2O) and N_2O yield (N_2O_{yield}) were quantified based on the $^{29}N_2$ (P_{29}), $^{30}N_2$ (P_{30}), $^{45}N_2O$ (P_{45}), and $^{46}N_2O$ (P_{46}) production rates from intact core incubations (Hsu and Kao, 2013; Risgaard-Petersen et al., 2003),

$$D_{14} = 2(r_{14}+1) \times r_{14} \times P_{30} + r_{14} \times (2P_{46} + P_{45}), \quad (7)$$

$$A_{14} = 2 \times r_{14} \times (P_{29} - 2 \times r_{14} \times P_{30}), \quad (8)$$

$$D_{14} - N_2O = r_{14} \times (P_{45} + 2P_{46}), \quad (9)$$

$$N_2O_{yield} = (D_{14} - N_2O/D_{14}) \times 100, \quad (10)$$

where r_{14} is calculated from production rates of $^{29}N_2$ and $^{30}N_2$, and the slurry incubation-based *ra*%,

$$r_{14} = \frac{(1 - ra\%) \times (P_{29}/P_{30}) - ra\%}{2 - ra\%}. \quad (11)$$

The total nitrogen removal rate (P_{14}) can be computed by summing genuine N_2 and N_2O production from denitrification and anammox,

$$P_{14} = D_{14} + A_{14} = 2r_{14} \times [P_{29} + (1 - r_{14}) \times P_{30}] + r_{14} \times (2P_{46} + P_{45}). \quad (12)$$

A parameter of $r_{14}w$, the ratio of $^{14}NO_3^-$ to $^{15}NO_3^-$ concentration in the overlying water, was introduced to separate direct denitrification (nitrogen removal supported by bottom-water-delivered NO_x^- *via* physical diffusion, $P_{14}w$) and coupled nitrification-denitrification (nitrogen removal supported by sedimentary nitrification produced NO_x^-, $P_{14}n$),

$$P_{14}w = P_{14} \times \frac{r_{14}w}{r_{14}}, \quad (13)$$

$$P_{14}n = P_{14} - P_{14}w. \quad (14)$$

2.7. Quantifying the capacity of sediment nitrogen removal and N_2O release

As the substrate for nitrogen removal processes, the correlations between *in situ* biogeochemical rates and bottom water NO_x^- concentration (X) follow the Michaelis-Menten kinetic, which were empirically fitted using a hyperbola equation with single rectangular and 2 parameters,

$$Y = \frac{a \times X}{b + X}, \tag{15}$$

where Y represents the site-specific areal rates of denitrification, anammox and denitrification-derived N_2O production; a and b are constants.

The spatial distribution of sedimentary denitrification, anammox and associated N_2O production rates in the whole PRE were then extrapolated according to the empirical formulas and bottom water NO_x^- concentration in 2021 (see details in following text). The PRE is zoned to 20 boxes based on the sampling stations (Supplementary Fig. S1), the nitrogen removal and N_2O emission fluxes (F) were then estimated,

$$F = \sum_{i=1}^{20} A_i \times \overline{R_i}, \tag{16}$$

where A_i and $\overline{R_i}$ represent the area and the average biogeochemical rates (denitrification, anammox and N_2O production) of the i^{th} box, respectively. Finally, the denitrification and anammox fluxes were summed up as the total nitrogen removal capacity in PRE sediments.

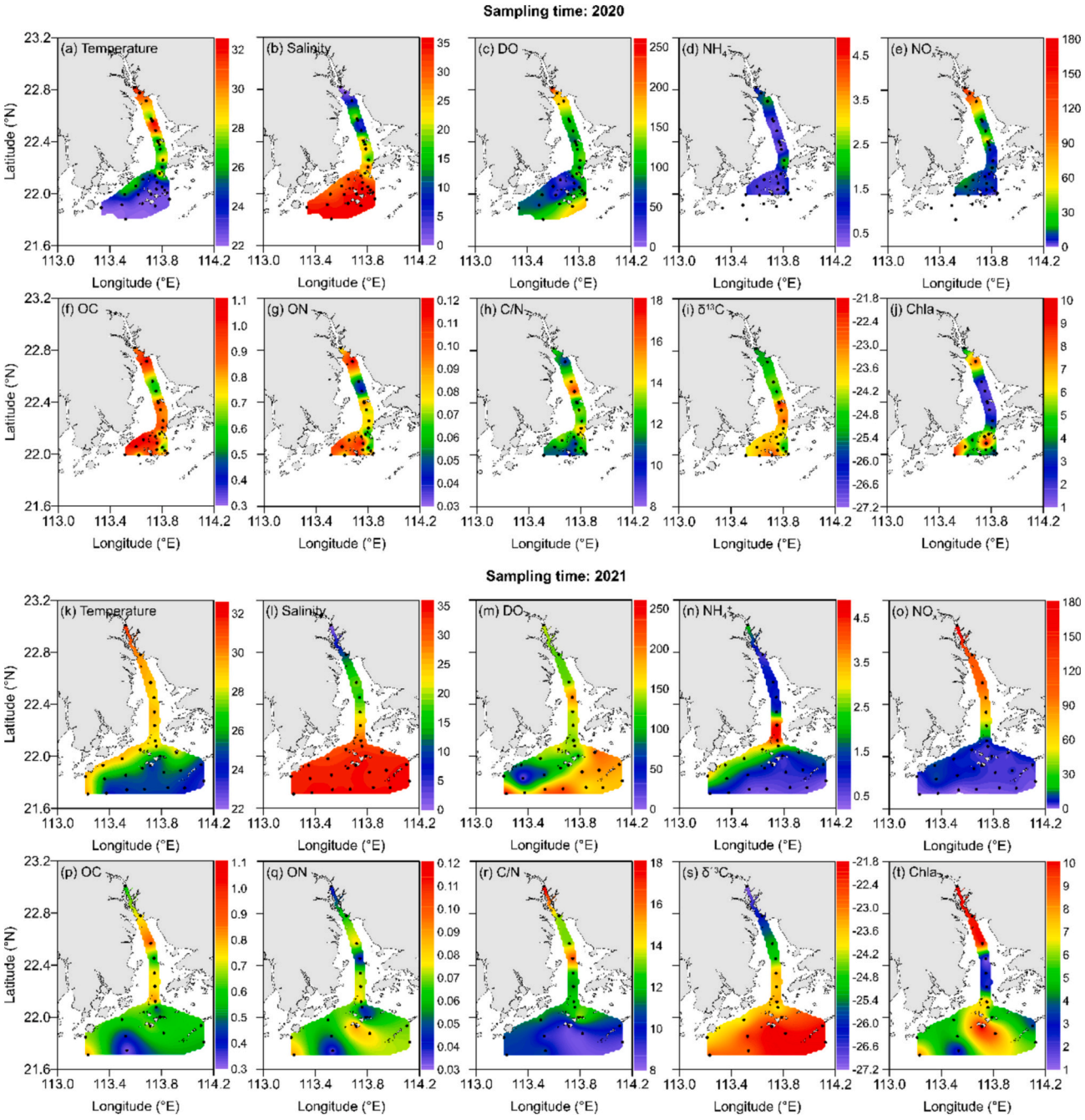

Fig. 2. The spatial distribution of fundamental parameters in bottom water (temperature, salinity, DO, NH_4^+ and NO_x^-) and surface sediments (OC, ON, C/N, $\delta^{13}C$, and Chla) of the Pearl River Estuary during the sampling time in (a-j) 2020 and (k-t) 2021.

2.8. Determination of content of marine sourced organic matter

The bulk C/N and organic $\delta^{13}C$ are effective indicators for sources of OM in estuarine sediments (Yu et al., 2010). We applied a simple $\delta^{13}C$-based two endmember mixing model to further quantify the relative contribution of marine source to sediment OM (f_{marine}) in the PRE based on the following equation (Schultz and Calder, 1976):

$$f_{marine} = \frac{\delta^{13}C_{OC} - \delta^{13}C_{terr}}{\delta^{13}C_{marine} - \delta^{13}C_{terr}} \times 100\% \quad (17)$$

where $\delta^{13}C_{OC}$ is the measured $\delta^{13}C$ of sediment OM; $\delta^{13}C_{terr}$ and $\delta^{13}C_{marine}$ represent the endmember of terrestrial and marine OM, here were taken as 28.3 ‰ and 19.4 ‰, respectively (Su et al., 2017). Then the content of marine sourced OM was calculated by multiplying the bulk OM and f_{marine}.

2.9. Statistical analysis

Pearson's correlation was applied to test the correlations between nitrogen removal rates and different environmental variables. All statistical analyses were conducted at a 0.05 significance level using Statistical Package of Social Sciences (SPSS, version-19.0). The data fittings were conducted applying SigmaPlot 12.5 software.

3. Results

3.1. Environmental settings

In general, the temperature and salinity of bottom water ranged from 22 to 31 °C (Fig. 2a and k) and 0–34 (Fig. 2b and l) during the two sampling campaigns, respectively. DO concentration in bottom water varied from 17 to 248 μmol L^{-1} (Fig. 2c) and 64–257 μmol L^{-1} (Fig. 2m) in 2020 and 2021, respectively. NH_4^+ concentration in 2020 ranged from 0.3 to 2.2 μmol L^{-1} with a small spatial heterogeneity (Fig. 2d); In 2021, NH_4^+ concentration was relatively higher (2.7–4.7 μmol L^{-1}) in the middle of the estuary than that in the inner and outer estuary (Fig. 2n). NO_x^- dominated the dissolved inorganic nitrogen species in the bottom water and presented a decreasing pattern seaward with concentrations of 2.5–138.8 μmol L^{-1} in 2020 (Fig. 2e) and of 0.5–178.6 μmol L^{-1} in 2021 (Fig. 2o).

The sedimentary OC and ON contents varied from 0.6 to 1.1 % and 0.04–0.12 % in 2020, respectively (Fig. 2f and g). While their contents were relatively lower in 2021 with a range of 0.3–0.9 % for OC (Fig. 2p) and 0.03–0.09 % for ON (Fig. 2q). The C/N spanned from 9.8 to 17.0 and from 8.6 to 18.3 during 2020 and 2021, respectively, with relative lower values in the outer estuary (Fig. 2h and r). The $\delta^{13}C$ of sediment OM increased gradually seaward with a range of −25.4 ‰ to −21.7 ‰ in 2020 (Fig. 2i) and − 27.1 ‰ to −21.9 ‰ in 2021 (Fig. 2s). The concentration of Chla in surface sediments ranged from 1.7 to 9.7 μg g^{-1} in 2020 (Fig. 2j) and from 1.1 to 10.6 μg g^{-1} in 2021 (Fig. 2t), with lower concentration observed in the middle estuary.

3.2. Sediment oxygen consumption rates

The SOC rates in the PRE ranged from 56.1 to 69.9 mmol O_2 m^{-2} d^{-1} (with an average of 63.4 ± 6.9 mmol O_2 m^{-2} d^{-1}) and from 22.5 to 65.1 mmol O_2 m^{-2} d^{-1} (with an average of 47.3 ± 14.2 mmol O_2 m^{-2} d^{-1}) during 2020 and 2021, respectively (Fig. 3).

3.3. Potential rates of sedimentary nitrogen removal and associated N_2O production

The potential rates of sedimentary denitrification varied from 9.1 to 71.2 nmol N mL^{-1} h^{-1} in 2020 (31.5 ± 17.3 nmol N mL^{-1} h^{-1}; Fig. 4a) and from 3.0 to 160.6 nmol N mL^{-1} h^{-1} in 2021 (54.5 ± 47.4 nmol N mL^{-1} h^{-1}; Fig. 4f). Spatially, denitrification presented relative lower potential rates in the middle estuary than those in the upper and lower estuary (Fig. 4a and e). Among the detected environmental factors, denitrification potential rates were negatively correlated to sediment C/N and positively correlated to sediment Chla concentration (Table 1). The potential anammox rates were 1–2 orders of magnitude lower than those of denitrification with a range of 3.6–20.4 nmol N mL^{-1} h^{-1} (Fig. 4b) in 2020 and 0.5–9.7 nmol N mL^{-1} h^{-1} (Fig. 4f) in 2021. The positive correlations were observed between anammox potential rates and bottom water Chla, sediment OC and ON contents (Table 1). The contribution of anammox to total Nr loss decreased spatially from upper to lower estuary with a range of 14.9–34.2 % (23.5 ± 5.0 %; Fig. 4c) and 1.0–29.5 % (11.8 ± 8.4 %; Fig. 4g) during the investigation in 2020 and 2021, respectively.

N_2O was an important product during nitrogen removal in the PRE sediments, showing a similar spatial distribution pattern to denitrification with potential rates of 1.2–17.9 nmol N mL^{-1} h^{-1} (average 8.0 ± 5.0 nmol N mL^{-1} h^{-1}, Fig. 4d) in 2020 and 1.1–40.1 nmol N mL^{-1} h^{-1} (average 15.3 ± 11.8 nmol N mL^{-1} h^{-1}, Fig. 4h) in 2021. The low potential N_2O production rates were mainly observed in the middle estuary regardless of the sampling time. The N_2O production potential rates showed positive correlations to bottom water NH_4^+ concentration and sediment Chla content (Table 1). The potential N_2O yield varied from 5.4 to 52.1 % in 2020 and 11.7–52.3 % in 2021, with averages of 20.6 ± 11.8 % and 30.0 ± 12.1 %, respectively (Fig. 4e and j). Negative correlations were observed between potential N_2O yield and the contents of OC and ON (Table 1).

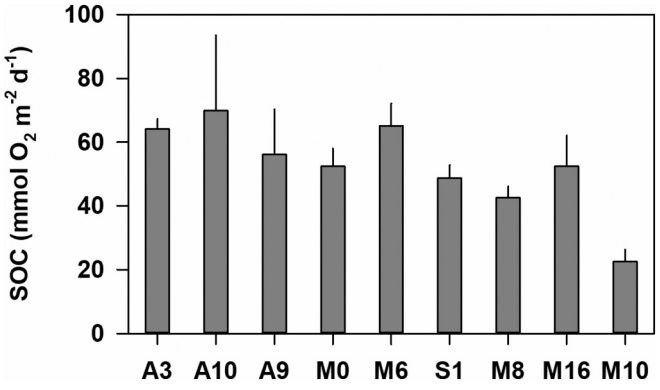

Fig. 3. The sediment oxygen consumption rates from two sampling campaigns in the PRE. The error bars denote the standard deviation of triplicates.

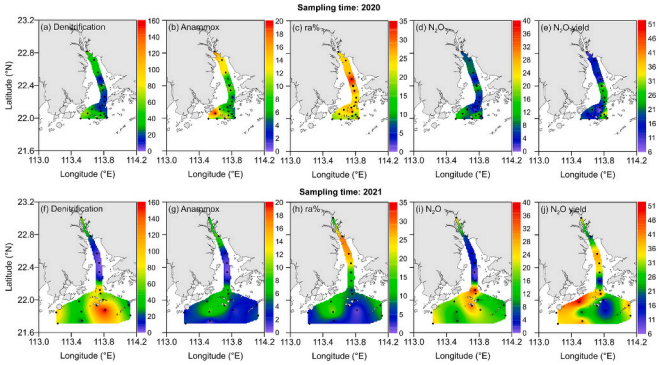

Fig. 4. The spatial distribution of potential biogeochemical rates (denitrification, anammox and N_2O production) and proportions (ra% and N_2O yield) in Pearl River Estuary during the sampling in (a-e) 2020 and (f-j) 2021.

Table 1
Pearson's correlation coefficients between nitrogen removal potential rates and environmental factors. Data points from the two investigations ($n = 39$) are assembly presented. Bold and underlined numbers denote statistically significant correlations ($p < 0.05$).

Factors		D_{total}	A_{total}	ra%	N_2O_{total}	N_2O yield
Bottom water properties	T	−0.004	0.035	0.020	0.024	−0.016
	S	0.210	−0.233	**−0.365**	0.219	0.201
	NO_x^-	−0.160	0.110	0.224	−0.152	−0.040
	NH_4^+	0.220	−0.217	**−0.346**	**0.347**	0.245
	Chla	−0.042	**0.384**	0.055	−0.031	−0.022
Surface sediment properties	OC	−0.082	**0.476**	**0.477**	−0.171	**−0.309**
	ON	0.136	**0.415**	0.214	−0.028	**−0.318**
	C/N	**−0.334**	−0.047	**0.342**	−0.178	0.132
	Chla	**0.486**	0.101	−0.229	**0.435**	−0.149
	Porosity	0.181	0.155	0.086	0.102	−0.177

Note that T and S denote the bottom water temperature and salinity, respectively.

3.4. *In situ* benthic nitrogen loss and associated gaseous production rates

In spatial, the *in situ* rates of denitrification, anammox, N_2O production, direct denitrification and coupled nitrification-denitrification showed a decrease pattern from upstream to downstream in the PRE regardless of the sampling time (Fig. 5). The *in situ* denitrification rates ranged from 47.8 to 193.1 μmol N m^{-2} h^{-1} (average 108.4 ± 75.6 μmol N m^{-2} h^{-1}) in 2020 and from 5.6 to 208.6 μmol N m^{-2} h^{-1} (average 52.1 ± 78.4 μmol N m^{-2} h^{-1}) in 2021 (Fig. 5a), with a negative correlation to salinity and a positive correlation to bottom water NO_x^- concentration (Table 2). By contrast, the *in situ* anammox rates varied from 13.9 to 65.0 μmol N m^{-2} h^{-1} and 0.1–20.2 μmol N m^{-2} h^{-1}, with an average of 38.6 ± 25.6 μmol N m^{-2} h^{-1} and 4.6 ± 7.9 μmol N m^{-2} h^{-1}, accounting for 26.1 ± 4.1 % and 6.0 ± 3.4 % of the total benthic nitrogen loss in 2020 and 2021, respectively (Fig. 5a). Both *in situ* anammox rate and its contribution to total Nr removal showed positive correlations to sediment OC and ON contents (Table 2). N_2O was produced with rates of 0.02–0.2 μmol N m^{-2} h^{-1} (average 0.07 ± 0.08 μmol N m^{-2} h^{-1}) in 2020 and 0.1–7.1 μmol N m^{-2} h^{-1} (average 1.7 ± 2.7 μmol N m^{-2} h^{-1}) in 2021, accounting for 0.02–0.08 % (0.05 ± 0.03 %) and 1.4–16.6 % (4.9 ± 5.8 %) of denitrification, respectively (Fig. 5b). Averagely, denitrification directs 3.3 ± 5.2 % of removed nitrogen to N_2O loss regardless of the spatiotemporal variation. The *in situ* N_2O production rates were negatively correlated to salinity, but positively correlated to NO_x^- concentration in bottom water and C/N in sediment (Table 2).

The nitrogen removal rates supported by water-column-delivered NO_x^- (direct denitrification, $P_{14}w$) varied from 7.0 to 197.8 μmol N m^{-2} h^{-1} in 2020 and 0.6–187.6 μmol N m^{-2} h^{-1} in 2021 (Fig. 5c). Significant correlations were observed between direct denitrification and bottom water salinity and NO_x^- concentration (Table 2). The coupled nitrification-denitrification ($P_{14}n$) ranged from 54.6 to 84.5 μmol N m^{-2} h^{-1} and 4.5–50.6 μmol N m^{-2} h^{-1} in 2020 and 2021, respectively (Fig. 5c). The coupled nitrification-denitrification rates were tightly correlated to OC content and SOC rate (Table 2). The coupled nitrification-denitrification predominated the sediment Nr removal pathway in the PRE, with an increasing proportion from upstream to downstream, averagely contributing to 60.5 ± 33.6 % and 75.9 ± 28.8 % in 2020 and 2021, respectively (Fig. 5c). While in the fresh water side corresponding to the regions with high bottom water NO_x^- concentration (sites A3 and M0), physical diffusion of NO_x^- from water column play a more significant role in sustaining sedimentary nitrogen removal.

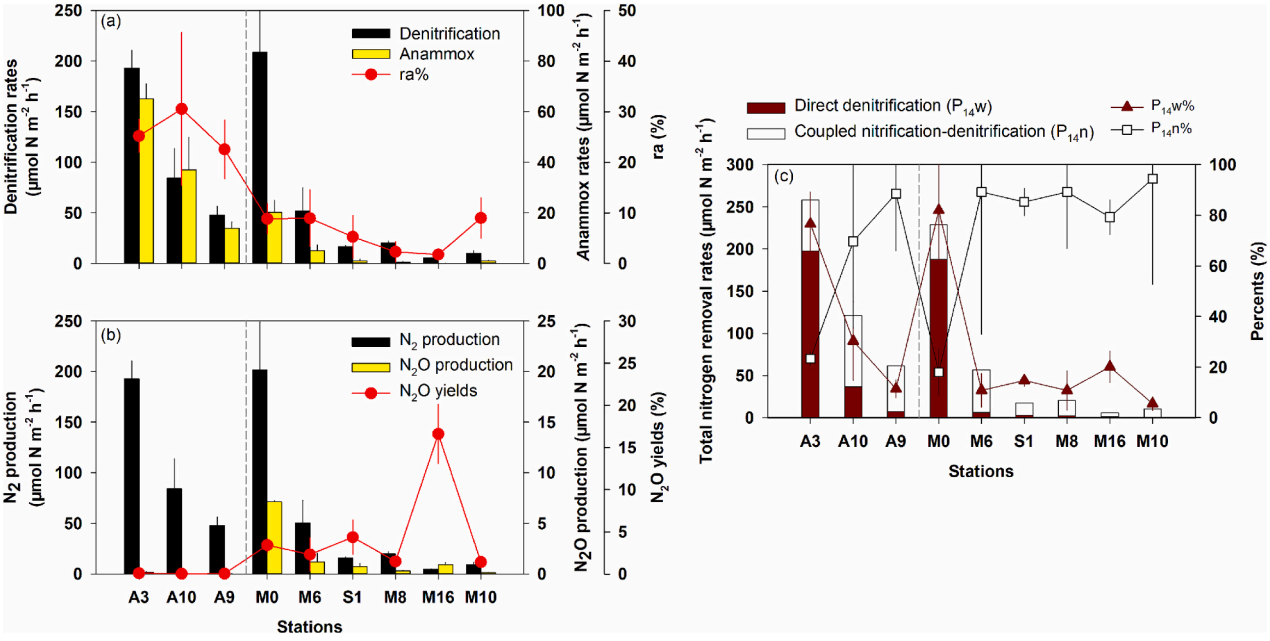

Fig. 5. The spatial distribution of *in situ* nitrogen removal and associated gaseous production rates in the PRE sediments. (a) denitrification, anammox, and the relative contribution of anammox (ra%) to total nitrogen removal; (b) denitrification-derived N_2 and N_2O production; (c) the nitrogen loss supported by water-column-delivered nitrate ($P_{14}w$) and sedimentary coupled nitrification-denitrification ($P_{14}n$), and the proportional contribution of individual processes to total nitrogen removal. The station sites were ordered from upstream to downstream. The error bar represents the standard deviation of triplicates. Note that the results from two sampling campaigns in 2020 and 2021 were separated by dotted lines.

Table 2
Pearson's correlation coefficients between *in situ* nitrogen removal rates and environmental factors. Data points from the two investigations ($n = 9$) are assembly presented. Bold and underlined numbers denote statistically significant correlations ($p < 0.05$).

Factors		Denitrification	Anammox	ra%	Direct denitrification	Coupled nitrification-denitrification	N_2O production	N_2O yield
Bottom water properties	T	0.523	0.171	−0.367	0.606	−0.194	0.616	0.424
	S	**−0.944**	−0.605	0.142	**−0.972**	−0.258	**−0.706**	0.142
	NO_x^-	**0.903**	0.453	0.096	**0.904**	0.223	**0.864**	−0.109
	NH_4^+	0.006	−0.163	−0.382	0.001	−0.122	0.216	0.486
	Chla	0.181	0.019	0.196	0.115	0.188	0.446	0.390
Surface sediment properties	OC	0.446	**0.804**	**0.791**	0.365	**0.830**	−0.275	−0.292
	ON	0.142	**0.675**	**0.709**	0.114	0.612	−0.601	−0.303
	C/N	0.593	0.028	−0.127	0.528	0.126	**0.922**	0.079
	Chla	0.605	0.408	0.133	0.547	0.409	0.476	−0.275
	Porosity	0.382	0.583	0.458	0.411	0.327	−0.152	−0.498
	SOC	0.435	0.576	0.571	0.310	**0.778**	0.019	−0.08

Note that T and S denote the bottom water temperature and salinity, respectively. SOC represents the sediment oxygen consumption rate.

4. Discussion

4.1. Spatial distribution of marine-sourced organic matter in surface sediment

The relative contribution of marine source to sediment OM presents a seaward increase pattern and the marine sourced OM constitutes more than half of sediment OM in the middle to outer estuary during both sampling time (Fig. 6a and c). The content of marine-sourced OC varied from 0.2 to 0.7 % and 0.1–0.5 % in 2020 and 2021, with averages of 0.4 ± 0.1 % and 0.3 ± 0.1 %, respectively (Fig. 6b and d). The marine-sourced OM is mainly produced through local phytoplankton photosynthesis, it is thus labile and easily utilized by microbes (Liu and Xue, 2020). Such a result indicates that primary production in water column plays a critical role in supplying LOM in the PRE sediments, subsequently sustaining the heterotrophic microbial activities, such as denitrification.

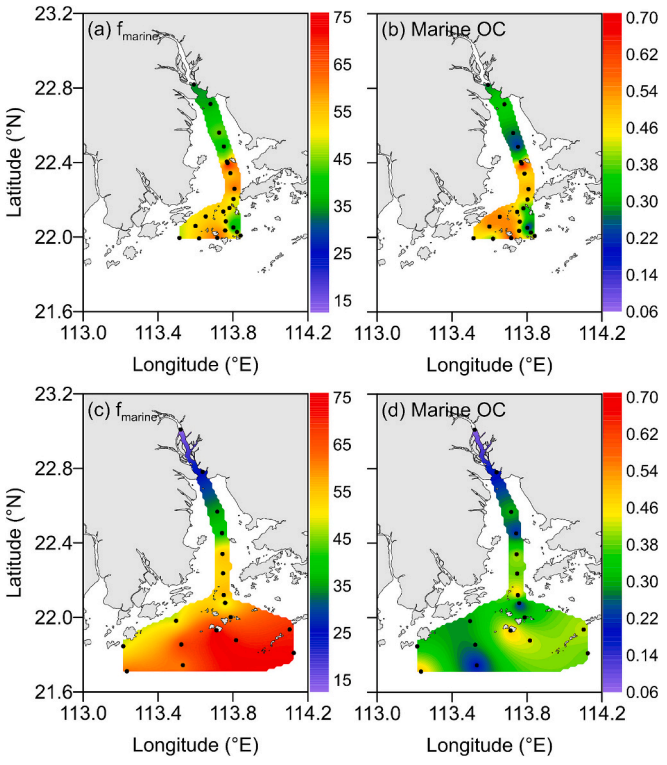

Fig. 6. The spatial distribution of f_{marine} and marine-sourced OC content in surface sediments of PRE in (a and b) 2020 and (c and d) 2021.

4.2. LOM stimulates sedimentary Nr removal and reduces N_2O yield

Sedimentary denitrification surpasses anammox to predominate the Nr loss with a substantial product flow towards N_2O production in the PRE (Fig. 4 and Fig. 5). OM is one of the crucial environment factors affecting the capacity of sediment Nr removal and the associated N_2O release (Tables 1 and 2). Based on the results from slurry incubation, the denitrification potentials showed no significant correlations with sedimentary OC and ON contents (Table 1), suggesting that the quantity of OM is not a limiting factor for Nr removal potential. However, the significant and negative correlation between denitrification potentials and C/N ratio (Fig. 7a) implies that the LOM with low C/N ratio benefits to benthic denitrification. In addition, the low potential denitrification rates are spatially coupled to the low concentration of Chla in both water and sediments, particularly in the upper and middle estuary (Supplementary Fig. S2). Chla acts as a proxy of the LOM in the seafloor (Stephens et al., 1997). Denitrification potentials were positively correlated to sedimentary Chla concentration, f_{marine} and marine-sourced OC content (Fig. 7b-d), directly supporting that LOM stimulates the potential capacity of denitrification in estuarine sediments.

Moreover, the *in situ* rates of coupled nitrification-denitrification, the dominant Nr removal pathway, were significantly and positively correlated to the sedimentary OC contents, marine-sourced OC contents, the Chla concentration, and SOC rate (Fig. 7e-h). Such correlations suggest that LOM stimulates sediment Nr removal mainly by promoting the coupled nitrification- denitrification process. Integrating the potential and *in situ* results indicate that denitrification in the PRE is highly depended on the content of LOM in sediments. The regulation of LOM on sediment Nr removal was universal and our results agree well with other observations (Albert et al., 2021; Callbeck et al., 2021; Huang et al., 2022; Lai et al., 2022). On one hand, organic matter drives the microbially-mediated carbon and nitrogen biogeochemical processes by functioning as energy and substrate sources in aquatic sediments (Bartl et al., 2019; Happel et al., 2019). Particularly, LOM is usually easier to be degraded by heterotrophic microorganisms, and release more energy and nitrogen to fuel Nr removal microbes. On the other hand, sediment OM respiration consumes oxygen and creates suitable environmental conditions to support nitrification, denitrification, and their coupling (Albert et al., 2021).

For the denitrification-induced N_2O production in sediments, the content of OM showed no significant effects on the potential and *in situ* N_2O production rates (Tables 1 and 2). Interestingly, both the potential and *in situ* N_2O yields were negatively correlated to the OC and ON contents (Fig. 8a-d), indicating that abundant OM may lead to more removed nitrogen flow towards N_2 during sediment denitrification to reduce the N_2O proportion. To consolidate this finding, we compiled the limited data on the *in situ* N_2O yield and production rate, which was obtained by applying the intact core incubation in Jiulong River Estuary and Yangtze River Estuary (Tan et al., 2022). In this compilation, weak negative correlations were observed between *in situ* N_2O yield and OC/

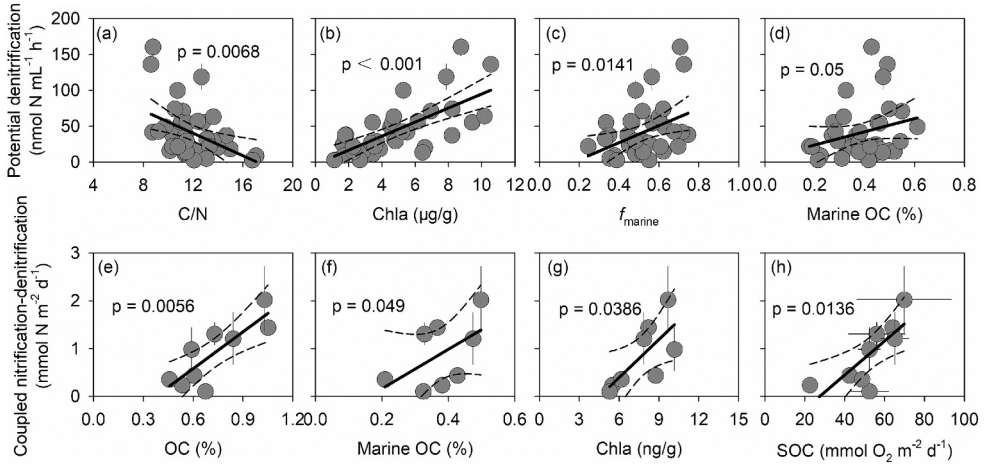

Fig. 7. The correlations between biogeochemical rates and sediment properties. The black line shows the linear fitting and dotted line denotes the 95 % confidence band. Error bar represents the standard deviation.

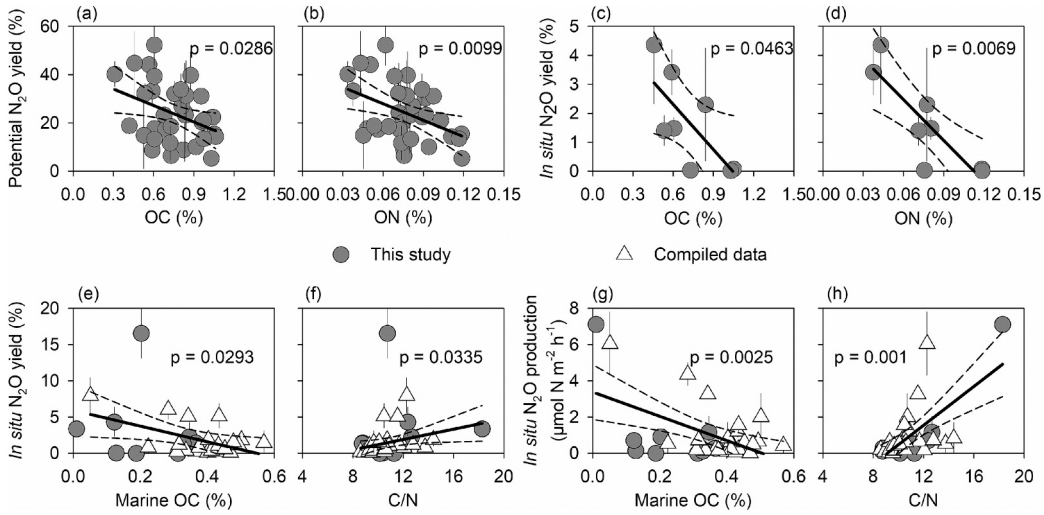

Fig. 8. The correlations between N_2O yield/production and sediment properties in this study and compiled data. The black line shows the linear fitting and dotted line denotes the 95 % confidence band. Error bar represents the standard deviation. Note that the extremely high value of *in situ* N_2O yield were excluded from the linear fitting in subfigures (c) and (d).

ON contents (Supplementary Fig. S3). However, the *in situ* N_2O yield and production rate were negatively correlated to marine-sourced OC (Fig. 8e and g) and positively correlated to C/N (Fig. 8f and h). These significant correlations further demonstrate that LOM stimulates N_2O consumption and then decreases N_2O yield. Since N_2O reduction is relatively a more energy consuming pathway than the other multiple enzymatic processes during denitrification (Richardson et al., 2009). High OM content, particularly LOM, produces more energy to accelerate N_2O reduction, that is, the complete denitrification, leading to a decrease in N_2O yield. This study is the first time to explore the environmental controls on sedimentary denitrification-derived N_2O production in aquatic ecosystems at both potential and *in situ* levels. Our results in estuarine environments were in line with the observations that organic carbon rich condition decreases the product stoichiometry of N_2O during denitrification in soil systems (Qin et al., 2017; Senbayram et al., 2012; Stuchiner and von Fischer, 2022). Lin et al. (2017) found that terrestrial OM increases the potential N_2O:N_2 ratio during sediment denitrification in East China Sea, which also supports our findings. However, more field data are needed in the future to confirm the effects of OM on N_2O production/consumption during sediment denitrification.

4.3. The regulation of nitrate on sedimentary Nr removal and associated N_2O production

We empirically fitted the *in situ* rates of sediment denitrification, anammox, and associated N_2O production to bottom water NO_x^- concentration following a hyperbola equation (Fig. 9a-c). Nitrate directly decides the spatial variability in Nr removal processes supported by direct denitrification *via* affecting physical diffusion of nitrate at the sediment-water interface. More importantly, nitrate serves as the major dissolved inorganic nitrogen species in the PRE (Fig. 2), and plays an important role in fueling primary productivity, that is the LOM production (Su et al., 2017; Xu et al., 2022), thereby influencing the LOM-driven coupled nitrification-denitrification in sediments. This may be a common phenomenon in estuaries around the world, as the compiled data clearly show that the sediment Nr removal rates present a similar nitrate-controlled trend to the PRE, regardless of the sampling time and regions (Fig. 9d). Such a trend indicates that sedimentary Nr removal rate increased rapidly and then reach to saturation with the increase of bottom water nitrate concentration in global estuaries, implying that future nutrient load increase will have slight effects on sediment Nr removal in the fresh water side, but significantly stimulate sediment Nr

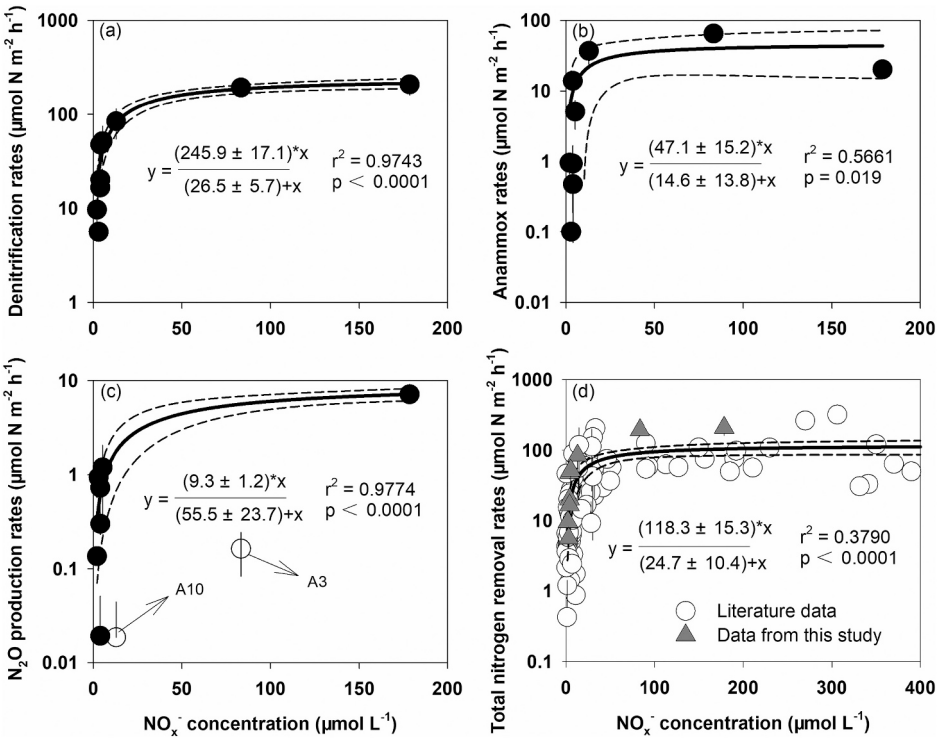

Fig. 9. The empirical fitting between biogeochemical rates and bottom water NO_x^- concentration based on the Michaelis-Menten kinetic. Data in panels (a)-(c) were from this study. Panel (d) shows a compilation data from global estuaries including this study. All data are listed in Supplementary Table S2. The black line shows the linear fitting and dotted line denotes the 95 % confidence band. The error bar represents the standard deviation.

removal in mid to lower estuaries, and even the outer shelf regions.

4.4. Quantification of Nr removal capacity and associated climatic feedback in the PRE

According to the empirical equations (Fig. 9a-c) and the bottom water NO_x^- concentration in 2021 (Fig. 2o), the spatial distribution of *in situ* denitrification, anammox and N_2O production rates are projected in the PRE (See details in Supplementary Fig. S4). Both the denitrification and anammox rates present a steep decreasing pattern from upper to lower estuary with a range of 0.10–5.14 mmol N m^{-2} d^{-1} and 0.03–1.04 mmol N m^{-2} d^{-1}, respectively (Supplementary Fig. S4a and b). As a dominant nitrogen removal pathway, the areal denitrification rates in the PRE are comparable to the field measurements in sediments from other estuaries, such as the Thames Estuary (Trimmer et al., 2006) (0.1–4.6 mmol N m^{-2} d^{-1}), Randers Fjord Estuary (Risgaard-Petersen et al., 2004) (1.9–8.0 mmol N m^{-2} d^{-1}), St. Lawrence Estuary (Crowe et al., 2012) (0.3 mmol N m^{-2} d^{-1}), Yangtze River Estuary (Yang et al., 2022) (0.3–6.3 mmol N m^{-2} d^{-1}) and Jiulong River Estuary (Tan et al., 2022) (0.5–2.6 mmol N m^{-2} d^{-1}), but are 1–2 orders of magnitude higher than the results of 0.03–0.50 mmol N m^{-2} d^{-1} in shelf sediments (Cheung et al., 2024; McTigue et al., 2016; Rysgaard et al., 2004). The total sediment Nr removal capacity in the PRE is estimated to be 1.1 ± 0.04 × 10^7 mol N d^{-1}, with 80.3 % and 19.7 % of contribution from denitrification (9.1 ± 0.3 × 10^6 mol N d^{-1}) and anammox (2.2 ± 0.3 × 10^6 mol N d^{-1}), respectively. The total bioavailable nitrogen including dissolved inorganic nitrogen and particulate organic nitrogen delivered into the PRE (Cai et al., 2015; He et al., 2010) is approximately 4.5 × 10^7 mol N d^{-1}, approximately 25.3 ± 1.0 % of the riverine inputted Nr is thus eliminated. These findings suggest that even though the PRE serves as a significant hotspot for Nr removal, however, nearly three quarters of riverine Nr load are exported into the offshore seas, resulting in biogeochemical and climatic feedbacks at a larger spatial scale.

Denitrification directs 0.002–0.17 mmol N m^{-2} d^{-1} of N_2O production in the PRE sediments (Supplementary Fig. S4c). The sedimentary N_2O production rates are in line with the findings from different estuaries (Dong et al., 2006; Salk et al., 2017; Tan et al., 2022; Wang et al., 2007; Yang et al., 2022) with a range of 0.001–0.27 mmol N m^{-2} d^{-1}. Similarly, the sedimentary denitrification-induced N_2O release flux was 2.4 ± 0.2 × 10^5 mol N d^{-1} in the whole PRE. Lin et al. (2016) has reported that the average areal rate of sea-air N_2O emission was 0.07 ± 0.03 mmol N m^{-2} d^{-1}. Applying the same study area (4750 km^2) in this study, the sedimentary denitrification-induced N_2O emission occupies 66.0 ± 27.3 % of the daily sea-air N_2O efflux in the PRE. Tan et al. (2022) has found that sedimentary N_2O production accounts for 58.7 % and 64.6 % of the sea-air N_2O flux in the Yangtze River Estuary and Jiulong River Estuary, respectively. Such findings strongly suggest that estuarine sediment acts as a significant N_2O source and may contribute greatly to the local and global climatic feedback.

5. Conclusions and perspectives

Sediment receives the local-produced LOM from water column, hosting a hotspot of aerobic respiration and then nitrate respiration to enhance Nr removal, resulting in environmental and climatic feedbacks. Accordingly, we reveal a universal mechanism of riverine Nr removal in estuarine sediment *via* primary production-LOM settling-sedimentary respiration-coupled nitrification-denitrification (Fig. 10). This chain processes link the carbon and nitrogen biogeochemical cycles in the atmosphere-water column-sediment continuum at different temporal and spatial scales (Fig. 10). LOM facilitates sediment Nr removal while reducing denitrification-induced N_2O yield and production rate (Fig. 10). However, the estuarine ecosystems play a weak role in purifying excess Nr input due to their limited area, short water residence time, high Nr loading and ultimately the low removal efficiency. The majority of riverine Nr is outflowed into the adjacent shelf seas to alleviate the offshore nitrogen limitation and promote the biological carbon pump, but also trigger offshore ecological issues. Based on these

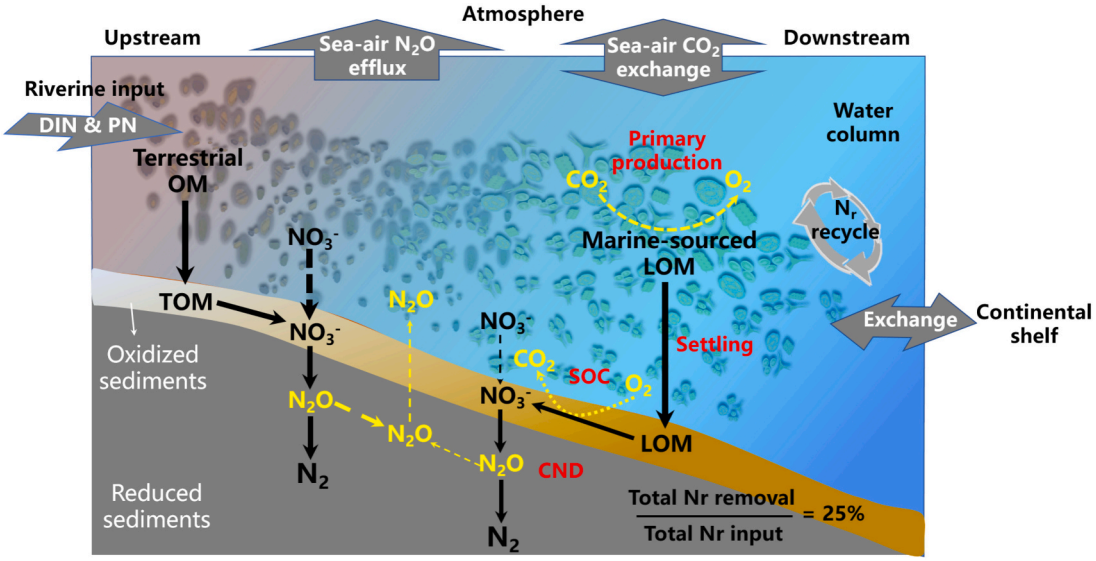

Fig. 10. The conceptual diagram illustrating the controls of organic matter and nitrate on the sediment nitrogen removal and N_2O yield. TOM and LOM represent terrestrial organic matter and labile organic matter, respectively. SOC is sediment oxygen consumption. CND denotes coupled nitrification-denitrification. The solid and dotted lines represent the sedimentation/biogeochemical and diffusion processes, respectively. The thickness of the arrow represents the relative size of rate/proportion.

scientific findings, we propose that reducing upstream Nr load to improve the net Nr removal efficiency and reduce N_2O production, and thus to achieve a sustainable development of the offshore ecosystems with a low climatic feedback. In the future, a series of measures should be taken to control the upstream nutrients load, including wastewater treatment capacity improvement (Strokal et al., 2015; Tong et al., 2020), land management (Borrelli et al., 2020), rational fertilization and fertilizer utilization efficiency improvement (Zhang et al., 2015). In addition, light is an important driving factor of LOM production in water column. Previous finding has indicated that estuarine turbidity suppress benthic Nr removal capacity *via* reducing light availability and the subsequent phytoplankton photosynthesis (Huang et al., 2022). Reducing the total suspended sediments transportation and improving the hydrodynamic power may also be important means to improve the Nr self-purification in estuaries.

CRediT authorship contribution statement

Ehui Tan: Writing – review & editing, Writing – original draft, Validation, Methodology, Investigation, Funding acquisition, Formal analysis, Data curation. **Bin Chen:** Writing – review & editing, Writing – original draft, Methodology, Investigation, Formal analysis. **Lili Han:** Writing – review & editing, Writing – original draft, Methodology, Investigation. **Wenbin Zou:** Writing – review & editing, Writing – original draft, Validation, Methodology, Investigation. **Xiuli Yan:** Writing – review & editing, Writing – original draft, Methodology, Investigation, Funding acquisition. **Zhixiong Huang:** Writing – review & editing, Writing – original draft, Methodology, Investigation. **Yu Han:** Writing – review & editing, Writing – original draft, Data curation. **Zhenzhen Zheng:** Writing – review & editing, Writing – original draft. **Liwei Zheng:** Writing – review & editing, Writing – original draft. **Min Xu:** Writing – review & editing, Writing – original draft. **Jin-Yu Terence Yang:** Writing – review & editing, Writing – original draft, Investigation. **Hongyan Bao:** Writing – review & editing, Writing – original draft. **Shuh-ji Kao:** Writing – review & editing, Writing – original draft, Supervision, Funding acquisition, Conceptualization.

Declaration of competing interest

The authors declare that they have no known competing financial interests or personal relationships that could have appeared to influence the work reported in this paper.

Acknowledgements

Special acknowledgment to intensive field and laboratory works by Li Tian and Yong Fang. This study was supported by the National Natural Science Foundation of China (#42276043, #92251306, #42306120, and # 42176046). Hainan Provincial Natural Science Foundation of China (#623RC456). Innovational Fund for Scientific and Technological Personnel of Hainan Province (#KJRC2023B04). Collaborative Innovation Center of Marine Science and Technology in Hainan University (#XTCX2022HYC19). We are grateful to anonymous reviewers for their constructive comments. The data that support the findings of this study are available on request from the corresponding author.

Appendix A. Supplementary data

Supplementary data to this article can be found online at https://doi.org/10.1016/j.marpolbul.2024.117190.

Data availability

Data will be made available on request.

References

Albert, S., et al., 2021. Influence of settling organic matter quantity and quality on benthic nitrogen cycling. Limnol. Oceanogr. 66 (5), 1882–1895.
Bartl, I., et al., 2019. Particulate organic matter controls benthic microbial N retention and N removal in contrasting estuaries of the Baltic Sea. Biogeosciences 16 (18), 3543–3564.
Beusen, A.H.W., et al., 2016. Global riverine N and P transport to ocean increased during the 20th century despite increased retention along the aquatic continuum. Biogeosciences 13 (8), 2441–2451.
Bohlen, L., et al., 2012. Simple transfer functions for calculating benthic fixed nitrogen losses and C:N:P regeneration ratios in global biogeochemical models. Global Biogeochem. Cycles 26 (3), GB3029.
Borrelli, P., et al., 2020. Land use and climate change impacts on global soil erosion by water (2015-2070). Proceedings of the National Academy of Sciences, USA 117 (36), 21994–22001.

Braman, R.S., Hendrix, S.A., 1989. Nanogram nitrite and nitrate determination in environmental and biological materials by vanadium (III) reduction with chemiluminescence detection. Anal. Chem. 61 (24), 2715–2718.
Cai, P., et al., 2015. Using $^{224}Ra/^{228}Th$ disequilibrium to quantify benthic fluxes of dissolved inorganic carbon and nutrients into the Pearl River estuary. Geochim. Cosmochim. Acta 170, 188–203.
Callbeck, C.M., et al., 2021. Anoxic chlorophyll maximum enhances local organic matter remineralization and nitrogen loss in Lake Tanganyika. Nat. Commun. 12 (1), 830.
Chen, B., et al., 2023. The external/internal sources and sinks of greenhouse gases (CO_2, CH_4, N_2O) in the Pearl River estuary and adjacent coastal waters in summer. Water Res. 249, 120913.
Cheng, X., et al., 2023. Shifts in the high-resolution spatial distribution of dissolved N_2O and the underlying microbial communities and processes in the Pearl River estuary. Water Res. 243, 120351.
Cheung, H.L.S., et al., 2024. Denitrification, anammox, and DNRA in oligotrophic continental shelf sediments. Limnol. Oceanogr. 9999, 1–17.
Crowe, S.A., et al., 2012. Anammox, denitrification and fixed-nitrogen removal in sediments from the Lower St. Lawrence Estuary. Biogeosciences 9 (11), 4309–4321.
Dalsgaard, T., et al., 2000. Protocol Handbook for NICE Nitrogen Cycling in Estuaries. National Environmental Research Institute, Copenhagen, Denmark.
Dong, L.F., et al., 2006. Sources of nitrogen used for denitrification and nitrous oxide formation in sediments of the hypernutrified Colne, the nutrified Humber, and the oligotrophic Conwy estuaries, United Kingdom. Limnol. Oceanogr. 51 (1part2), 545–557.
Happel, E.M., et al., 2019. Effects of allochthonous dissolved organic matter input on microbial composition and nitrogen-cycling genes at two contrasting estuarine sites. FEMS Microbiol. Ecol. 95 (9), 1–10.
He, B., et al., 2010. Sources and accumulation of organic carbon in the Pearl River estuary surface sediment as indicated by elemental, stable carbon isotopic, and carbohydrate compositions. Biogeosciences 7 (10), 3343–3362.
Hsu, T.C., Kao, S.J., 2013. Technical note: simultaneous measurement of sedimentary N_2 and N_2O production and a modified ^{15}N isotope pairing technique. Biogeosciences 10 (12), 7847–7862.
Huang, F., et al., 2022. Effects of marine produced organic matter on the potential estuarine capacity of NO_x^- removal. Sci. Total Environ. 812, 151471.
Hutchins, D.A., Capone, D.G., 2022. The marine nitrogen cycle: new developments and global change. Nat. Rev. Microbiol. 1–14.
IPCC, 2021. Climate Change 2021: The Physical Science Basis. Contribution of Working Group I to the Sixth Assessment Report of the Intergovernmental Panel on Climate Change. Cambridge University Press, Cambridge, United Kingdom and New York, NY, USA (In press).
Jameson, B.D., et al., 2020. Continental margin sediments underlying the NE Pacific oxygen minimum zone are a source of nitrous oxide to the water column. Limnol. Oceanogr. Lett. 6 (2), 68–76.
Kao, S.J., et al., 2008. North Pacific-wide spreading of isotopically heavy nitrogen during the last deglaciation: evidence from the western Pacific. Biogeosciences 5 (6), 1641–1650.
Katz, B.G., 2020. Nitrogen Overload: Environmental Degradation, Ramifications, and Economic Costs. American Geophysical Union and John Wiley and Sons, Inc., Hoboken and Washington, D.C.
Kessouri, F., et al., 2021. Coastal eutrophication drives acidification, oxygen loss, and ecosystem change in a major oceanic upwelling system. Proceedings of the National Academy of Sciences, USA 118 (21), e2018856118.
Lai, X., et al., 2022. Nitrogen loss from the coastal shelf of the East China Sea: implications of the organic matter. Sci. Total Environ. 854, 158805.
Lin, H., et al., 2016. Spatiotemporal variability of nitrous oxide in a large eutrophic estuarine system: the Pearl River Estuary, China. Mar. Chem. 182, 14–24.
Lin, X., et al., 2017. Nitrogen losses in sediments of the East China Sea: spatiotemporal variations, controlling factors, and environmental implications. J. Geophys. Res. Biogeo. 122 (10), 2699–2715.
Liu, Z., Xue, J., 2020. The lability and source of particulate organic matter in the Northern Gulf of Mexico hypoxic zone. J. Geophys. Res. Biogeosci. 125 (9), e2020JG005653.
Liu, J.P., et al., 2009. Fate of sediments delivered to the sea by Asian large rivers: long-distance transport and formation of remote alongshore clinothems. Sedimentary Record 7 (4), 4–9.
Ma, P., et al., 2019. The isotopomer ratios of N_2O in the Shaying River, the upper Huai River network, eastern China: the significances of mechanisms and productions of N_2O in the heavy ammonia polluted rivers. Sci. Total Environ. 687, 1315–1326.
Mao, Q., et al., 2004. Tides and tidal currents in the Pearl River estuary. Cont. Shelf Res. 24 (16), 1797–1808.
McTigue, N.D., et al., 2016. Biotic and abiotic controls on co-occurring nitrogen cycling processes in shallow Arctic shelf sediments. Nat. Commun. 7, 13145.
Morley, N.J., et al., 2014. Substrate induced denitrification over or under estimates shifts in soil N_2/N_2O ratios. PloS One 9 (9), e108144.
Murray, R.H., et al., 2015. Nitrous oxide fluxes in estuarine environments: response to global change. Glob. Chang. Biol. 21 (9), 3219–3245.
Pai, S.C., et al., 2001. pH and buffering capacity problems involved in the determination of ammonia in saline water using the indophenol blue spectrophotometric method. Anal. Chim. Acta 434, 209–216.
Phillips, R.L., et al., 2015. Temperature effects on N_2O and N_2 denitrification end-products for a New Zealand pasture soil. N. Z. J. Agric. Res. 58 (1), 89–95.
Pinckney, J., et al., 1994. Comparison of high-performance liquid chromatographic, spectrophotometric, and fluorometric methods for determining chlorophyll a concentrations in estaurine sediments. J. Microbiol. Methods 19 (1), 59–66.
Qian, W., et al., 2022. Long-term patterns of dissolved oxygen dynamics in the Pearl River Estuary. J. Geophys. Res. Biogeosci. 127 (7), e2022JG006967.
Qin, S., et al., 2017. Irrigation of DOC-rich liquid promotes potential denitrification rate and decreases $N_2O/(N_2O+N_2)$ product ratio in a 0–2 m soil profile. Soil Biol. Biochem. 106, 1–8.
Qu, Z., et al., 2014. Excessive use of nitrogen in Chinese agriculture results in high $N_2O/(N_2O+N_2)$ product ratio of denitrification, primarily due to acidification of the soils. Glob. Chang. Biol. 20 (5), 1685–1698.
Ravishankara, A.R., et al., 2009. Nitrous oxide (N_2O): the dominant ozone-depleting substance emitted in the 21st century. Science 326 (5949), 123–125.
Richardson, D., et al., 2009. Mitigating release of the potent greenhouse gas N_2O from the nitrogen cycle-could enzymic regulation hold the key? Trends Biotechnol. 27 (7), 388–397.
Risgaard-Petersen, N., et al., 2003. Application of the isotope pairing technique in sediments where anammox and denitrification coexist. Limnol. Oceanogr. Methods 1, 63–73.
Risgaard-Petersen, N., et al., 2004. Anaerobic ammonium oxidation in an estuarine sediment. Aquat. Microb. Ecol. 36, 293–304.
Rysgaard, S., et al., 2004. Denitrification and anammox activity in Arctic marine sediments. Limnol. Oceanogr. 49 (5), 1493–1502.
Salk, K.R., et al., 2017. Unexpectedly high degree of anammox and DNRA in seagrass sediments: description and application of a revised isotope pairing technique. Geochim. Cosmochim. Acta 211, 64–78.
Schultz, D., Calder, J.A., 1976. Organic carbon $^{13}C/^{12}C$ variations in estuarine sediments. Geochim. Cosmochim. Acta 40, 381–385.
Senbayram, M., et al., 2012. N_2O emission and the $N_2O/(N_2O+N_2)$ product ratio of denitrification as controlled by available carbon substrates and nitrate concentrations. Agr Ecosyst Environ 147, 4–12.
Stephens, M.P., et al., 1997. Chlorophyll-a and pheopigments as tracers of labile organic carbon at the central equatorial Pacific seafloor. Geochim. Cosmochim. Acta 61 (21), 4605–4619.
Strokal, M., et al., 2015. Increasing dissolved nitrogen and phosphorus export by the Pearl River (Zhujiang): a modeling approach at the sub-basin scale to assess effective nutrient management. Biogeochemistry 125 (2), 221–242.
Stuchiner, E.R., von Fischer, J.C., 2022. Using isotope pool dilution to understand how organic carbon additions affect N_2O consumption in diverse soils. Glob. Chang. Biol. 28, 4163-4179.
Su, J., et al., 2017. Tracing the origin of the oxygen-consuming organic matter in the hypoxic zone in a large eutrophic estuary: the lower reach of the Pearl River estuary, China. Biogeosciences 14, 4085–4099.
Tan, E., et al., 2022. Quantitatively deciphering the roles of sediment nitrogen removal in environmental and climatic feedbacks in two subtropical estuaries. Water Res. 224, 119121.
Thamdrup, B., Dalsgaard, T., 2002. Production of N_2 through anaerobic ammonium oxidation coupled to nitrate reduction in marine sediments. Appl. Environ. Microbiol. 68 (3), 1312–1318.
Tian, H., et al., 2020. A comprehensive quantification of global nitrous oxide sources and sinks. Nature 586 (7828), 248–256.
Tong, Y., et al., 2020. Improvement in municipal wastewater treatment alters lake nitrogen to phosphorus ratios in populated regions. Proceedings of the National Academy of Sciences, USA 117 (21), 11566–11572.
Trimmer, M., et al., 2006. Direct measurement of anaerobic ammonium oxidation (anammox) and denitrification in intact sediment cores. Mar. Ecol. Prog. Ser. 326, 37–47.
Wan, X.S., et al., 2023. Particle-associated denitrification is the primary source of N_2O in oxic coastal waters. Nat. Commun. 14 (1), 8280.
Wang, D., et al., 2007. Summer-time denitrification and nitrous oxide exchange in the intertidal zone of the Yangtze estuary. Estuar. Coast. Shelf Sci. 73 (1–2), 43–53.
Wang, J., et al., 2020a. Spatially explicit inventory of sources of nitrogen inputs to the Yellow Sea, East China Sea, and South China Sea for the period 1970–2010. Earth's Future 8 (10), e2020EF001516.
Wang, R., et al., 2020b. Using field-measured soil N_2O fluxes and laboratory scale parameterization of $N_2O/(N_2O+N_2)$ ratios to quantify field-scale soil N_2 emissions. Soil Biol. Biochem. 148, 107904.
Xiang, H., et al., 2023. NosZ-II-type N_2O-reducing bacteria play dominant roles in determining the release potential of N_2O from sediments in the Pearl River estuary, China. Environ. Pollut. 329, 121732.
Xu, M.N., et al., 2022. Diel change in inorganic nitrogenous nutrient dynamics and associated oxygen stoichiometry along the Pearl River estuary. Water Res. 222, 118954.
Yang, J.-Y.T., et al., 2022. Sedimentary processes dominate nitrous oxide production and emission in the hypoxic zone off the Changjiang River estuary. Sci. Total Environ. 827, 154042.
Yu, F., et al., 2010. Bulk organic $\delta^{13}C$ and C/N as indicators for sediment sources in the Pearl River delta and estuary, southern China. Estuar. Coast. Shelf Sci. 87 (4), 618–630.
Zhang, S., et al., 2008. Recent changes of water discharge and sediment load in the Zhujiang (Pearl River) basin, China. Global and Planetary Change 60 (3–4), 365–380.
Zhang, W., et al., 2013. Surficial sediment distribution and the associated net sediment transport pattern in the Pearl River estuary, South China. Cont. Shelf Res. 61–62, 41–51.
Zhang, X., et al., 2015. Managing nitrogen for sustainable development. Nature 528 (7580), 51–59.
Zhou, J., et al., 2023. Effects of acidification on nitrification and associated nitrous oxide emission in estuarine and coastal waters. Nat. Commun. 14 (1), 1380.